Mon. Not. R. astr. Soc. (1992) **256,** 13–25

Waves in solar magnetic flux tubes: the observational signature of undamped longitudinal tube waves

S. K. Solanki[1] and B. Roberts[2]

[1] *Institute of Astronomy, ETH-Zentrum, CH-8092 Zürich, Switzerland*
[2] *The Mathematical Institute, University of St Andrews, St Andrews, Fife, KY16 9SS*

Accepted 1991 November 20. Received 1991 November 18; in original form 1991 June 13

SUMMARY

Linear calculations of undamped longitudinal waves in thin solar magnetic flux tubes are presented. The influence of such waves, having a variety of parameters, on the Stokes I and V profiles of eight photospheric spectral lines is studied. Diagnostics based on the Stokes parameters of the properties of flux tube waves, in particular of the amount of energy transported by them into the upper solar atmosphere, are developed. For propagating waves we find that, with an appropriate choice of spectral lines, a lower limit on the transported energy can be set by observing the zero-crossing wavelength of Stokes V, while an upper limit can be derived from the line-widths. The importance of radiative transfer effects and of the thermodynamic changes associated with the waves are pointed out. In particular, it is shown that waves with short wavelengths should not give rise to a large oscillation of the Stokes V zero-crossing wavelength, although they produce very asymmetric and broad line profiles. Some qualitative comparisons with the observational data are considered. It is shown that observations with sufficiently high spatial and temporal resolution should be able to distinguish between standing and propagating waves on the basis of line parameters of photospheric spectral lines alone.

The influence of flux tube waves on spatially and temporally unresolved observations is also considered. It is found that only downwards propagating linear tube waves produce the correct sign of the Stokes V asymmetry. Furthermore, linear tube waves cannot simultaneously reproduce the observed amplitude and area asymmetry of the Stokes V line profiles, even in the presence of a downflow outside the flux tubes. This suggests that either longitudinal waves in solar magnetic flux tubes behave non-linearly, or that the thin-tube approximation breaks down.

1 INTRODUCTION

The existence of a rich variety of wave modes in solar magnetic flux tubes is expected from theoretical and physical considerations (*cf.* reviews by Spruit & Roberts 1983; Roberts 1984, 1986; Thomas 1985; Ryutova 1990). Such waves are expected to play an important role in heating the solar chromosphere and the corona (Wentzel 1974; Hollweg 1982; Heyvaerts & Priest 1983; Herbold *et al.* 1985; Hassler *et al.* 1990). Although acoustic waves in principle carry sufficient energy to heat the spatially averaged chromosphere (Anderson & Athay 1989), the tight correlation between the energy losses in chromospheric lines like Ca II H and K and the magnetic flux (Skumanich *et al.* 1975; Schrijver *et al.* 1989) suggests a magnetic origin of a sizeable fraction of the chromospheric heating. Longitudinal tube waves (also called sausage-mode waves) and the flux tube kink mode are the main candidates for magnetic chromospheric heating. So far, investigations of waves in flux tubes have concentrated either on the purely magnetohydrodynamic (MHD) aspects, which have been dealt with in great detail by various authors (e.g. Defouw 1976; Ryutov & Ryutova 1976; Roberts & Webb 1978, 1979; Webb & Roberts 1980; Spruit 1981; Rae & Roberts 1982; Herbold *et al.* 1985; Musielak, Rosner & Ulmschneider 1989; Ferriz-Maz, Schüssler & Anton 1989), or on the purely observational aspects (Giovanelli *et al.* 1978; Wiehr 1985; Solanki 1986, 1989; Fleck 1991). To our knowledge, only a single attempt has so far been made to combine the two approaches quantitatively: Rammacher & Ulmschneider (1989) have investigated the influence of longitudinal tube waves on the profiles of Ca II and Mg II spectral lines. Consequently, we have only a rough qualitative

idea of the observational signature of flux tube waves in photospheric spectral lines.

In the present paper we investigate the influence of longitudinal flux tube waves on photospheric line profiles, in particular on circularly polarized Stokes V profiles which are the main carriers of information on the spatially unresolved magnetic elements or small flux tubes (Stenflo 1989). We hope to identify the observations best suited to derive information on flux tube waves. We do not attempt to reproduce quantitatively the observations at this stage, restricting ourselves to qualitative comparisons. In Section 2 we list the assumptions and give a brief description of the methods with which we have calculated the waves and the Stokes profiles. The results are presented and discussed in Section 3 and our conclusions are outlined in Section 4. A preliminary version of a part of the work described here has been presented in Solanki & Roberts (1990).

2 MHD AND RADIATIVE TRANSFER ASPECTS

2.1 Description of the hydromagnetics

The basic assumptions of the model developed here are the following. (i) The flux tube structure is described by a thin-tube approximation (Defouw 1976; Roberts & Webb 1978, 1979; Parker 1979; Schüssler 1990; Roberts 1990). This assumption has been shown to agree very well with models including magnetic tension (Knölker, Schüssler & Weisshaar 1988; Steiner & Pizzo 1989) and with observations (Zayer, Solanki & Stenflo 1989). (ii) The waves are linear. (iii) The gas inside the flux tube is assumed to be uncoupled from the field-free surroundings, so that the calculated tube waves do not excite disturbances in the field-free atmosphere surrounding the flux tube. Note, however, that the present calculations do take into account the elasticity of the flux tube. (iv) Spatial radiative damping is neglected in the present paper.

For the calculation of a longitudinal tube wave under the assumptions listed above, the following differential equation for the normalized velocity, Q, must be solved (see Roberts & Webb 1978 for a derivation):

$$\frac{d^2Q}{dz^2}+\left[\frac{\omega^2-\Omega^2(z)}{c_{\rm T}^2}\right]Q=0. \tag{1}$$

Here $Q(z)$ is related to the local longitudinal velocity, v_1, of the oscillations due to the wave by

$$Q(z)=\sqrt{\frac{\rho_0(z)A_0(z)\,c_{\rm T}^2(z)}{\rho_0(0)A_0(0)c_{\rm T}^2(0)}}\,v_1(z), \tag{2}$$

where $\rho_0(z)$ is the gas density and $A_0(z)$ is the cross-sectional area of the flux tube at height z in the atmosphere (the height scale has been chosen such that $z=0$ corresponds to $\tau_{5000}=1$ in the quiet Sun). The tube speed $c_{\rm T}(z)$ is defined by

$$c_{\rm T}^2=c_{\rm s}^2v_{\rm A}^2/(c_{\rm s}^2+v_{\rm A}^2), \tag{3}$$

where $c_{\rm s}(z)=(\gamma p_0/\rho_0)^{1/2}$ is the sound speed and $v_{\rm A}(z)=B_0/(4\pi\rho_0)^{1/2}$ is the Alfvén speed within the flux tube. Here γ is the ratio of heat capacities and p_0 is the gas pressure. Throughout this text a subscript zero denotes quantities related to the undisturbed, stationary atmosphere, while subscript unity denotes linearized perturbations of atmospheric parameters caused by the wave.

The velocity amplitude $v_1(z)$ is related to the time-dependent longitudinal velocity $v_1(z,t)$ by

$$v_1(z,t)=\Re[v_1(z)\exp i\omega t], \tag{4}$$

where $\Re$ denotes the real part of a complex quantity. In the above ω is the frequency of the wave and $\Omega(z)$ depends only on variables of the undisturbed atmosphere:

$$\Omega^2=c_{\rm T}^2\left\{\frac{1}{2}(\ln\zeta)''+\frac{1}{4}[(\ln\zeta)']^2+\frac{g}{c_{\rm s}^2}\left[\left(\ln\frac{\zeta}{c_{\rm s}^2}\right)'+\frac{g}{c_{\rm s}^2}\right]\right\}$$
$$-g\left[(\ln\rho_0)'+\frac{g}{c_{\rm s}^2}\right], \tag{5}$$

where

$$\zeta=\gamma p_0B_0^3(4\pi\gamma p_0+B_0^2). \tag{6}$$

In the above, primes denote derivatives with respect to z, g is the acceleration due to gravity and B is the magnetic field strength.

Once ω is prescribed, equation (1) can be solved numerically. One of the main problems faced when solving equation (1) is the accurate calculation of the derivatives in equation (5) if ρ_0 and p_0 are taken from a tabulated solar atmospheric model. High accuracy is required since the various terms of Ω^2 have a similar magnitude and cancellation is common. We have obtained such accuracy by smoothing and interpolating between the data points prior to differentiation, using an extended version of the scheme proposed by Godratt, Greenfield & Schlesinger (1977).

Expressions for the total gas pressure, $p(z,t)$, which combines the pressure of the static medium and the perturbation, and the similarly defined total density, $\rho(z,t)$, etc., read:

$$p(z,t)=p_0(z)$$
$$+\Re\left[-i\left(\frac{\rho_0\{[g-c_{\rm s}^2(\ln A_0)']v_1-c_{\rm s}^2v_1'\}}{(1+c_{\rm s}^2/v_{\rm A}^2)\omega}\exp i\omega t\right]\right.$$
$$=p_0(z)+p_1(z,t), \tag{7}$$

$$\rho(z,t)=\rho_0(z)$$
$$-\Re\left[-i\left\{\frac{p_1(z,t)}{v_{\rm A}^2}-\frac{\rho_0}{\omega}[v_1'+(\ln\rho_0)'v_1+(\ln A_0)'v_1]\right\}\right.$$
$$\left.\times\exp i\omega t\right]=\rho_0(z)+\rho_1(z,t), \tag{8}$$

$$B(z,t)=B_0(z)-\frac{4\pi}{B_0}p_1(z,t), \tag{9}$$

$$A(z,t)=A_0(z)+\frac{A_0}{\rho_0v_{\rm A}^2}p_1(z,t), \tag{10}$$

$$T(z,t)=T_0(z)+\frac{mp_1(z,t)-RT_0\rho_1(z,t)}{R\rho_0}, \tag{11}$$

where m is the mean molecular weight. In accordance with

observations (Stenflo & Harvey 1985; Solanki 1986) we choose the unperturbed medium within the flux tube to be static.

Although we may solve equation (1) numerically for an arbitrary stratification of the unperturbed atmosphere, we have restricted attention to the case of an isothermal atmosphere. Such an assumption is common to investigations of the influence of acoustic waves on line profiles (e.g. Gomez *et al.* 1987). It removes complications arising from the fact that in a more realistic atmosphere the temperature and the vertical temperature gradient change considerably with height, thus affecting Ω, which in turn affects k, so that the wavelengths of the calculated waves depend strongly on height. In some cases $\omega^2-\Omega^2$ may even change sign, so that a wave with frequency ω may be propagating at one height but evanescent at another. This behaviour not only complicates the numerics considerably, but probably also is an artefact of the linear approximation (Schüssler, private communication). However, a truly non-linear calculation, which includes the reaction of the wave on the underlying temperature structure of the atmosphere, is not appropriate to the exploratory nature of the present investigation.

As the most important contribution to obtaining sufficiently realistic line profiles, the zeroth-order quantities p_0, B_0, etc. occurring in equations (2) and (7)–(15) are taken from a realistic model atmosphere, either the HSRA (Gingerich *et al.* 1971) or the network flux tube model of Solanki (1986). Thus the line profiles are formed in realistic, empirically derived atmospheres perturbed by a linear wave and may be directly compared with observations. The ambient, non-magnetic atmosphere is always described by the HSRA.

In an isothermal atmosphere c_T and Ω are independent of height, so that equation (1) has simple harmonic oscillatory and exponential solutions. We briefly write out these solutions, since they can be easily visualized. For propagating waves the velocity $v_1(z)$ may be written as

$$v_1(z)=v_1(0)\exp\left(\frac{z}{4H_0}\right)\exp(-ikz)=f_1(z)\exp(-ikz). \quad (12)$$

Here H_0 is the height-independent pressure scaleheight, k is the (real) wavenumber, $k^2=(\omega^2-\Omega^2)/c_T^2$, with $\omega^2>\Omega^2$. Thus, k is positive for upwards propagating waves and negative for downwards propagating waves. For evanescent waves ($\omega^2<\Omega^2$), k is imaginary: $k=-i|k|$.

Introducing equation (11) into equations (4), (7) and (8), we obtain

$$v(z,t)=f_1(z)\cos(\omega t-kz), \quad (13)$$

$$p(z,t)=p_0(z)+\frac{\rho_0\{[g-c_s^2(\ln A_0)']f_1-c_s^2f_1'\}}{(1+c_s^2/v_A^2)\,\omega}\sin(\omega t-kz)$$

$$+\frac{\rho_0kc_s^2f_1}{\omega(1+c_s^2/v_A^2)}\cos(\omega t-kz)=p_0(z)+p_1(z,t), \quad (14)$$

$$\rho(z,t)=\rho_0(z)-\frac{p_1(z,t)}{v_A^2}-\frac{\rho_0}{\omega}[f_1'+(\ln\rho_0)'f_1+(\ln A_0)'f_1]$$

$$\times\sin(\omega t-kz)+\frac{\rho_0kf_1}{\omega}\cos(\omega t-kz)$$

$$=\rho_0(z)+\rho_1(z,t). \quad (15)$$

Equations (9)–(11) for B, A and T remain formally unchanged, but $p_1(z,t)$ and $\rho_1(z,t)$ must be taken from equations (14) and (15), respectively. For propagating waves the phase difference between v and the other hydromagnetic variables is influenced by gravity and the wavenumber k. Also, p, ρ and T do not have the same phase. For a gravity-free atmosphere, i.e. for $g=0$, the phase difference between temperature and velocity, $\Delta\phi=0°$ (i.e. upwards flowing gas is hotter for an upwards propagating wave). The exact phase relationships have important consequences for the line profiles.

For a standing wave, we can write the total velocity as

$$v(z,t)=2f_1(z)\cos(kz)\cos(\omega t)=v_1(z)\cos(\omega t). \quad (16)$$

The sign of k now plays no role.

Finally, the velocity of an evanescent wave (imaginary k, i.e. $\omega^2<\Omega^2$) can be written as

$$v(z,t)=f_1(z)\exp(-|k|z)\cos(\omega t)=v_1(z)\cos(\omega t). \quad (17)$$

By introducing the expressions for $v_1(z)$ from equations (16) and (17) into equations (7) and (8), it is easy to write out explicitly the expressions for $p(z,t)$ and $\rho(z,t)$ for standing and evanescent waves. It follows from equations (7)–(11) and (16)–(17) that for standing waves and evanescent waves, p, ρ, B, T and A oscillate $\pm90°$ out of phase with the velocity. The general properties of longitudinal tube waves turn out to be relatively similar to those of acoustic waves.

Figs 1(a) and (b) show the velocity and temperature stratifications, respectively, at five phases of a propagating wave with a wavelength of 300 km and an amplitude of $v_1(z=0)=1.0$ km s^{-1} at $z=0$. We have chosen $\gamma=1.25$.

The squared amplitude of the wave increases considerably less rapidly with height than the density decreases and therefore also less rapidly than the squared amplitude of an acoustic wave in a plane-parallel atmosphere. For example, the density decreases by a factor of 20 between $z=0$ and 400 km, while the tube wave amplitude increases by only a factor of 2. This effect, which was previously noticed by Roberts & Webb (1978) and Herbold *et al.* (1985), is due to the rapid expansion with height of the flux tube, whose cross-sectional area increases approximately five-fold between $z=0$ and 400 km.

Finally, note that since the wave amplitude increases with height, the perturbation in T at $\tau=1$ in the tube is considerably smaller than at the heights of line formation (typically $\tau\approx10^{-2}$). Therefore, we can in general explain the behaviour of the line profiles by considering only the local values of T, v, etc., and neglecting perturbations in the continuum intensity.

2.2 Summary of the Stokes radiative transfer

To calculate the Stokes profiles we first produce snapshots of the atmosphere at various times (typically 10–12 per full wave period). From the resulting tables of $v(z)$, $p(z)$, $T(z)$, etc., the electron density, $p_e(z)$, the continuum absorption coefficient, $\kappa(z)$, and the continuum optical depth, $\tau(z)$, are calculated with the help of the code of Gustafsson (1973).

Since in the present paper we are primarily interested in basic effects and not in a direct comparison with the data, we

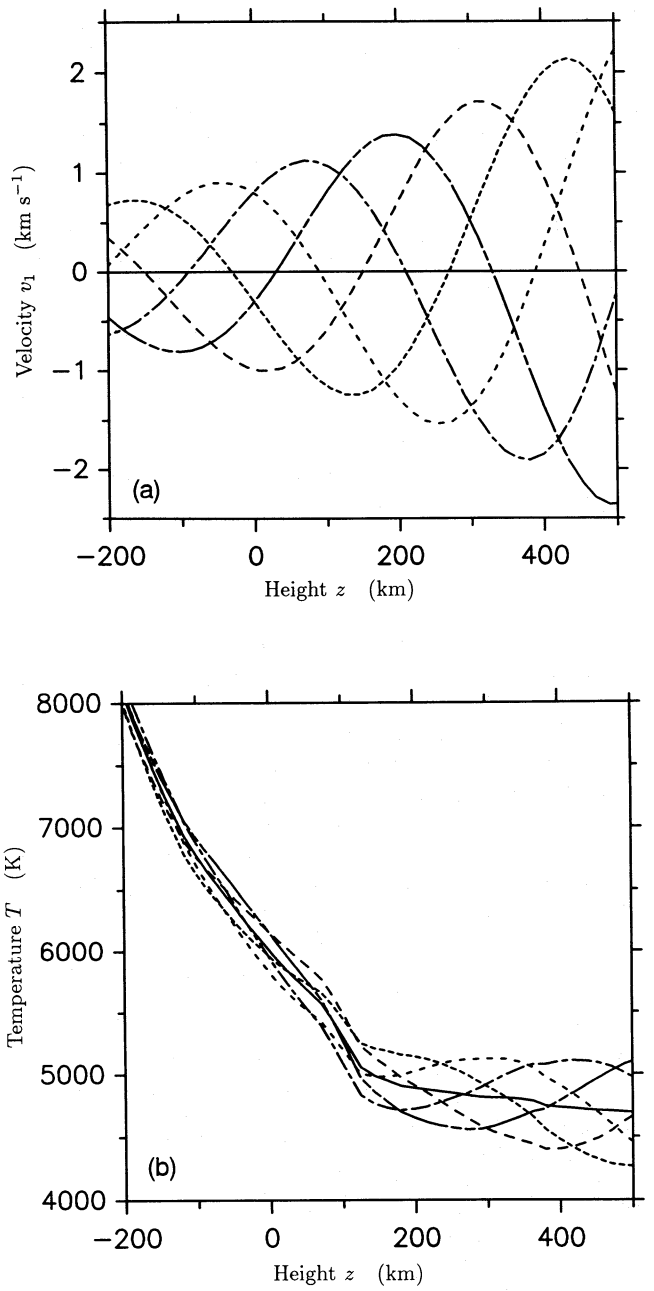

Figure 1. (a) Snapshots at five equidistant times, covering a full wave period, of the velocity, v_1, as a function of height, z, of a propagating wave. (b) Snapshots of the total temperature, T, as a function of z. The stationary empirical flux tube atmosphere (network flux tube model of Solanki 1986) on which the wave is superimposed is marked by the solid curve.

have not calculated specific lines present in the solar spectrum, but have chosen to use hypothetical lines of Fe I and II. These can be selected to give an optimum coverage of the line strength, excitation potential and Landé factor ranges with a minimum number of lines. The chosen lines include a weak, a medium-strong and a relatively strong low-excitation Fe I line, as well as a high-excitation Fe I and an Fe II line, which have been calculated for all the MHD models. A further three lines have only been calculated for selected models. All the hypothetical lines have a wavelength of 5000 Å. Further particulars of the lines are given in Table 1. The Stokes profiles are calculated using a Local Thermodynamic Equilibrium (LTE) code corresponding largely to the one described by Solanki (1987), which is based on a code by Beckers (1969).

Table 1. Calculated spectral lines.

Line No.	Ion	W_λ (mÅ)	χ_e (eV)	g
1	Fe I	55	0	1
2	Fe I	15	0	1
3	Fe I	110	0	1
4	Fe I	55	4	1
5	Fe II	55	3	1
6	Fe I	55	0	3
7	Fe I	15	4	1
8	Fe II	15	3	1

Horizontal perturbations (due to the elasticity of the flux tube) by a longitudinal tube wave, as estimated from equation (10), are $\lesssim 25$ per cent compared to the perturbations in the vertical direction. Therefore, longitudinal tube waves are not expected to provide a sizeable signal near the solar limb and cannot explain the large linewidths observed there by Pantellini, Solanki & Stenflo (1988). Accordingly, the calculations presented here are restricted to vertical flux tubes at solar disc centre and we need only discuss Stokes I (the unpolarized spectrum) and Stokes V (the difference between right-hand and left-hand circularly polarized light) profiles. The influence of the waves is quantified by considering, in addition to complete line profiles, specific line parameters like wavelengths, linewidths and asymmetries.

A total of approximately 90 waves have been calculated and their influence on the Stokes profiles analysed. The calculated waves have different periods, amplitudes, γ values, etc., and include standing waves, upwards and downwards propagating waves, pure sine waves, etc. Stokes I and V profiles have been calculated along the ray corresponding to the flux tube axis for all waves. In selected cases multiray calculations have been performed. These line profile calculations take the expansion of the flux tube with height explicitly into account by performing the transfer along multiple vertical rays passing through the flux tube at various distances from its axis of symmetry. In contrast to earlier multiray calculations, the rays are laid such that they intersect the flux tube boundary at regular *vertical* intervals. For vertical thin flux tubes at solar disc centre, this scheme achieves a comparable accuracy to the traditional scheme of horizontally equidistant intervals with less than half the number of rays. Typically 8–10 rays have been used. Various tests show that except for a few line parameters (notably the Stokes V asymmetry and wavelength shift) the single-ray models produce Stokes V profiles which are similar to the multiray ones. This is in agreement with previous investigations, which were, however, restricted to stationary atmospheres (e.g. Solanki 1989; Keller *et al.* 1990).

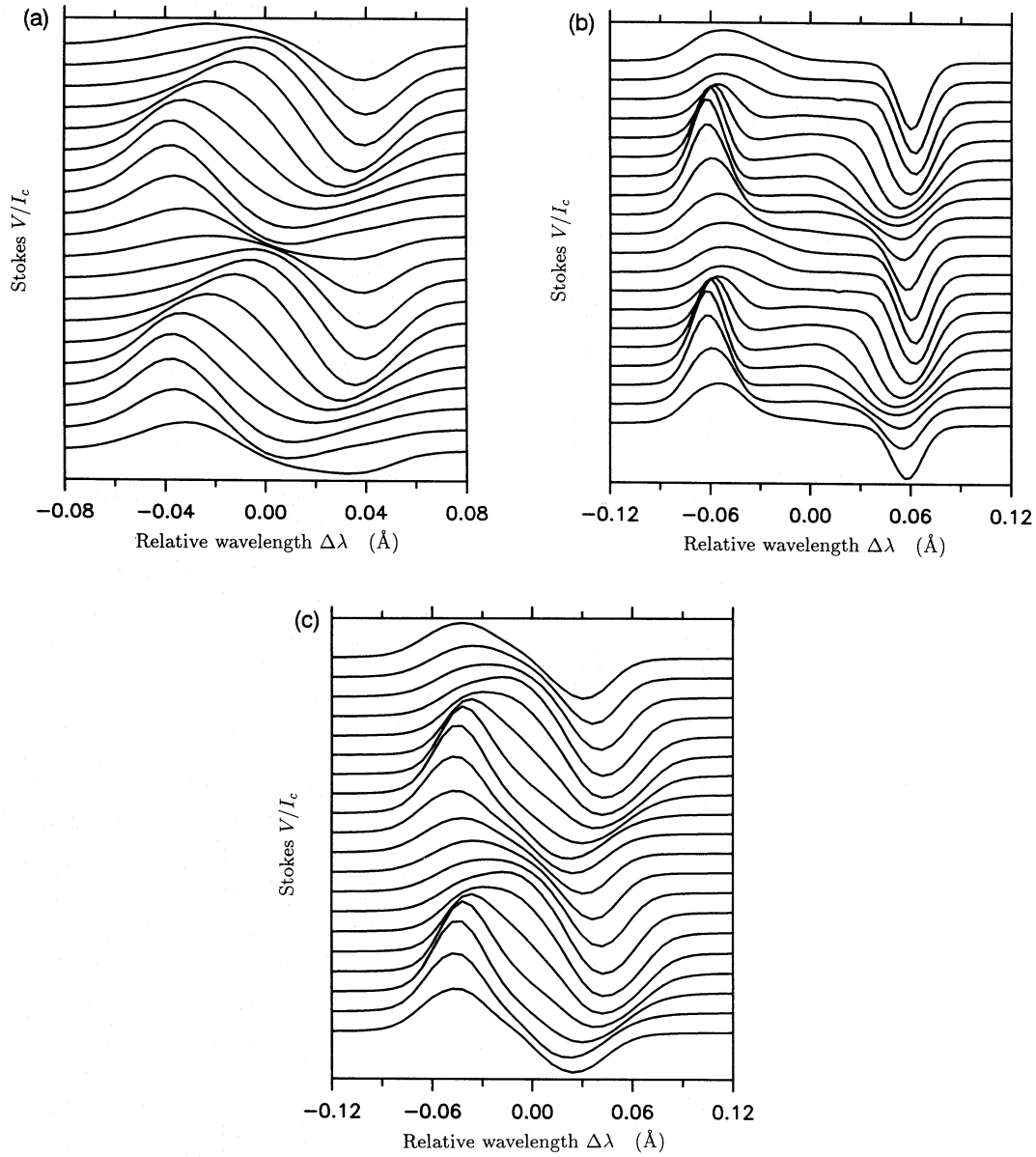

Figure 2. Snapshots of Stokes V profiles normalized to the local continuum intensity, I_c, in the presence of a propagating longitudinal flux tube wave with a wavelength of 300 km and $v_1(z=0)=1$ km s^{-1}. The plotted interval covers two wave periods. Profiles formed at later times are shifted upwards by an amount proportional to the time lag. The Stokes V profiles are averaged over multiple rays passing through the flux tube. (1.5-D calculations). (a) Line 1 of Table 1 (medium-strong, low-excitation Fe I line). (b) Line 3 (strong, low-excitation Fe I line). (c) Line 5 (medium-strong Fe II line).

3 RESULTS AND DISCUSSION

3.1 Complete line profiles

In this section we present the evolution of the complete line profiles with time. A detailed discussion of the influence of the waves on individual line parameters is to be found in Sections 3.2–3.5.

To illustrate the variety of responses to a given wave (wavelength $\Lambda_w=300$ km, $v_1(z=0)=1$ km s^{-1}), snapshots at 20 different times (covering 2 full wave periods) of the Stokes V profiles of three lines are plotted in Fig. 2. The profiles are the result of multiray calculations assuming a filling factor of $\alpha=15$ per cent at $z=0$. This filling factor is typical of solar plages. Since we consider only cases corresponding to observations at solar disc centre, no superposition of flux tubes along the line of sight is present.

Line 1 (Fig. 2a) shows a strong dependence of Stokes V wing area on phase. None of the three wavelength parameters analysed, the wavelength of the blue peak, λ_b, of the red peak, λ_r, and of the zero-crossing, λ_ν, describes a sine curve. A slowly increasing redshift, coupled with steadily increasing Stokes V amplitudes and wing areas, is followed by a rapid bluewards shift accompanied by a loss of line strength. Note that this behaviour, which is reminiscent of a non-linear wave, is due to a purely linear wave. Lines 2 and 6 behave similarly, although there are considerable quantitative differences. The V profile of line 3 (Fig. 2b) shows the

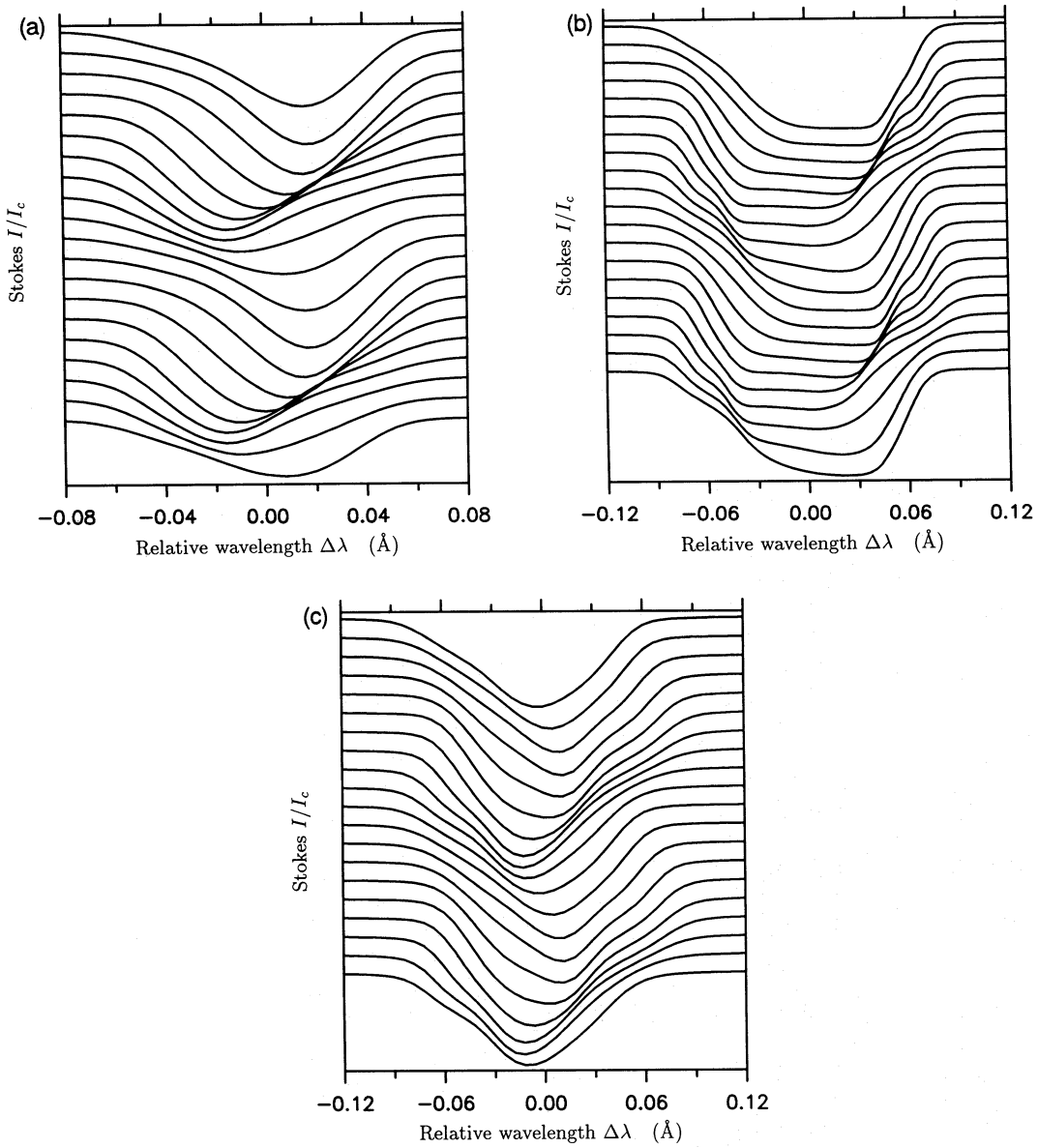

Figure 3. The same as Fig. 2, but showing the Stokes I/I_c profiles formed along the axis of the flux tube.

least obvious signs of the presence of a wave. Both λ_b and λ_r show only a weak oscillatory behaviour. The behaviour of λ_V is hard to judge, due to the extremely small gradient of the Stokes V profile near line centre.* The main effect of the wave appears to be on the asymmetry of the Stokes V profile of line 3, which changes dramatically with phase. Line 5 (Fig. 2c) shows in some respects the simplest behaviour. The wavelengths λ_b, λ_r and λ_V all appear to oscillate roughly sinusoidally and the line strength changes only slightly with phase. However, the line shape changes considerably. Lines 4, 7 and 8 (not plotted) behave qualitatively similarly. The dominant impression obtained from Fig. 2 is that longitudinal tube waves do not simply shift the lines, but also produce complex time-dependent changes in the line strength and shape. The changes in the various line parameters can have complex phase relationships.

Note that for standing waves and for propagating waves with $\gamma = 1$, all lines exhibit a behaviour similar to line 5, although line 3 still shows smaller wavelength fluctuations than the rest.

Synthetic Stokes I profiles formed along the axis of the tube (Fig. 3) simulate observations with extremely high spatial resolution ($\lesssim 0.1$ arcsec) as may become possible with future solar facilities. They also help us to understand the behaviour of the Stokes V profiles. The continuous strengthening of line 1 during the extended redshift phase, and its sudden weakening during the brief blueshift phase, are the dominant features of Fig. 3(a). Line 2 behaves similarly. The dominant feature of line 3 (Fig. 3b) is the almost time-independent shape and position of the strongly saturated line

*The flatness of Stokes V near line centre is *not* due to a large Zeeman splitting, but rather to a flat core of the Stokes I profile and a small splitting, due to $V \sim dI/d\lambda$. Note that no turbulence broadening velocity has been used.

core. The largest influence of the wave is seen in the line flanks. Since the Stokes V signal is strongest in the line flanks this also explains why for this line Stokes V shows much greater relative variations than Stokes I. Finally, line 5 (Fig. 3c) shows relatively little variation in line strength and its core wavelength describes an approximate sine curve, but the line shape is complex and changes as a function of time. In general the evolution of the Stokes I and of the Stokes V profiles is very similar.

The Stokes I profiles, averaged over the expanding tube out to a radius corresponding to $\alpha = 15$ per cent at $z = 0$, show little sensitivity to longitudinal tube waves. As a diagnostic of flux tube waves they are of little use and are not considered further in the present paper.

3.2 Zero-crossing wavelength

The measurement of the zero-crossing shift of Stokes V as a function of time is the classical way of looking for flux tube waves. Let us consider what observations with very high spatial resolution are expected to show.

Fig. 4 shows $\Delta\lambda_V$, the zero-crossing wavelength shift of Stokes V (in km s^{-1}), versus ωt (in degrees) for lines 1, 5 and 6. ω is the wave frequency and t is the time. Portrayed is the influence of a wave propagating upwards with $v_1(z=0)=1$ km s^{-1} and a wavelength of 300 km. Note that the different heights of formation of the cores of the three lines are reflected by the different times at which the largest redshifts for the various lines occur. Consequently, it should in principle be possible to distinguish between propagating waves and standing waves or oscillations, and possibly even to deduce propagation velocities, from high spatial resolution observations of purely photospheric spectral lines. Of course, by including chromospheric lines in the observed sample, the delay between the $\Delta\lambda_V$ responses of the various

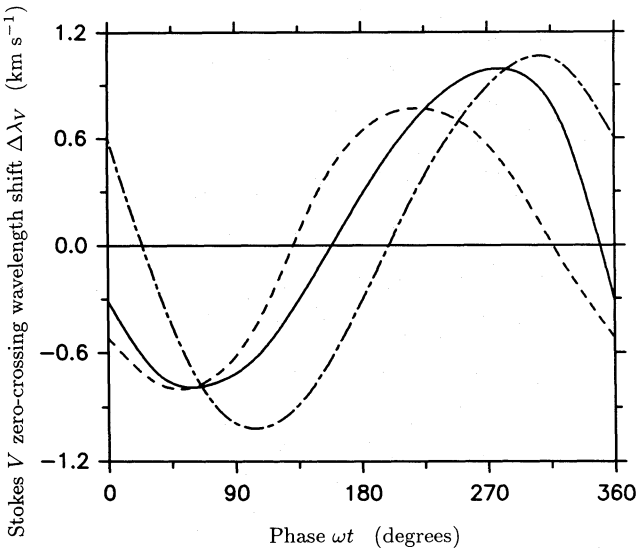

Figure 4. Zero-crossing wavelength shift $\Delta\lambda_V$ (in km s^{-1}) of synthetic Stokes V profiles versus phase or the product of wave frequency and time, ωt. The figure covers a full period of a propagating wave with a wavelength of $\lambda_w = 300$ km and an amplitude $v(z=0)=1$ km s^{-1}. Solid curve: line 1, dashed curve: line 5, dot-dashed curve: line 6 (like line 1, but with a Landé factor of 3).

Table 2. Amplitude of the oscillatory component of the Stokes V zero-crossing shift.

Line No.	$\Delta\lambda_V^{max}$ (km s^{-1}) for λ_w = 900 km	$\Delta\lambda_V^{max}$ (km s^{-1}) for λ_w = 300 km	$\Delta\lambda_V^{max}$ (km s^{-1}) for λ_w = 150 km
1	1.25	1.00	0.20
2	1.20	0.90	0.20
4	1.05	0.70	0.25
5	1.05	0.80	0.35

lines should increase and simplify the determination of the propagation velocity. There are practical problems, however. Consider Fig. 2(b), showing the strong line 3. The central part of the Stokes V profile is so flat that it is completely impractical to determine λ_V from observations (noise). For stronger (e.g. chromospheric) lines, the line core is broader still and λ_V should also be difficult to determine accurately.

The amplitudes $\Delta\lambda_V^{max}$ of the oscillations of the Stokes V zero-crossing wavelength, produced by three propagating waves with different wavelengths Λ_w, are given in Table 2. $\Delta\lambda_V^{max}$ decreases by up to a factor of 6 as Λ_w decreases from 900 to 150 km, although $v_1(z)$ remains unchanged. This implies that the energy flux transported by flux tube waves can easily be underestimated by a large factor (30–40 for $\Lambda_w = 150$ km) when derived from direct observations of wavelength shifts, if no corrrection is made for radiative transfer effects. For waves with the same Λ_w, but with larger amplitudes, the possible underestimate of the energy flux is even larger (*cf.* the discussion of Fig. 5, below).

Another possible method of detecting tube waves is to measure time series of λ_b or λ_r. For example, for line 3 this gives a small, but considerably more reliable signal of the wave than λ_V. For line 6, $\lambda_{b,r}$ show a considerably smaller variation than λ_V, while for the rest of the lines $\Delta\lambda_V^{max}$ and $\Delta\lambda_{b,r}^{max}$ are relatively similar. For propagating waves, there is generally a phase lag between $\lambda_{b,r}$ and λ_V, due to the different heights of formation of the two.

Spectral smearing, caused by, e.g., the finite spectral resolution of the instrument, also affects the response of λ_V to the wave. Since λ_V is shifted in the direction of the weaker Stokes V wing by spectral smearing (Solanki & Stenflo 1986) and since the blue Stokes V wing tends to dominate when λ_V is more strongly blueshifted (see Section 3.5), $\Delta\lambda_V^{max}$ decreases with increasing spectral smearing. For a Gaussian instrumental profile with an e-folding width less than approximately 120 mÅ, $\Delta\lambda_V^{max}$ decreases by up to a factor of 2–3. For line 3, we find that a certain amount of spectral smearing actually makes it easier to measure $\Delta\lambda_V(t)$, since for the line $dV/d\lambda$ at $\lambda = \lambda_V$ initially increases with increasing smearing, before decreasing again. However, we caution that after spectral smearing the interpretation of $\lambda_V(t)$ is no longer straightforward, since it is now also contaminated by the changing V asymmetry, and cannot be considered a reliable direct indicator of $v_1(z)$. For strong lines, it is probably better to measure the fluctuating Stokes V asymmetry directly (Section 3.5), or possibly concentrate on the wavelength, amplitude or width of a single Stokes V wing (*cf.* Fig. 2b). The effect of a Gaussian macroturbulent velocity distribution is, of course, identical to that of spectral smearing.

From the calculations described above, we conclude that measurements of $\lambda_V(t)$ can only be used to set a *lower limit* on the mechanical energy flux due to longitudinal tube

waves. The tightest such limit should be achieved by observing not too strong temperature-insensitive lines (e.g. weak Fe II lines).

The behaviour of $\Delta\lambda_V$ as a function of time and the value of $\Delta\lambda_V^{\max}$ are determined by four parameters of the waves: the velocity amplitude $v_1(z)$ of the wave, its wavelength Λ_w, the amplitude of the temperature fluctuations [set by $v_1(z)$ and γ] and finally the phase lag between the temperature and the velocity fluctuations. We have tested the relative importance of these and other parameters for $\lambda_V(t)$ by varying each wave parameter individually. The direct influence of $v_1(z=0)$ is obvious and need not be discussed further. Λ_w only plays a role when it is smaller than approximately twice the width of a typical Stokes V contribution function (see, e.g., Van Ballegooijen 1985; Grossmann-Doerth, Larsson & Solanki 1988a, for definitions of the Stokes V contribution function). Then the wave broadens the Stokes V profile more than it shifts it. Therefore, as λ_w decreases $\Delta\lambda_V^{\max}$ is expected to decrease. The calculations confirm these expectations (see Table 2). A similar effect for Stokes I is well known (e.g. Deubner 1976; Keil & Marmolino 1986).

The influence of temperature fluctuations is determined both by their amplitude and by their phase difference to v_1, $\Delta\phi$. The temperature fluctuations of evanescent or standing waves hardly affect $\lambda_V(t)$, since $\Delta\phi = 90°$. For undamped upwards propagating waves, $\Delta\phi$ is closer to 0°, so that temperature-sensitive lines weaken during the upflowing phase and strengthen during the downflowing phase, leading to a reduction of $\Delta\lambda_V^{\max}$ and a redshift of the line (averaged over a full oscillation period). The alternate strengthening and weakening is particularly evident for line 1 in Figs 2(a) and 3(a), but is hardly visible for the temperature-insensitive line 5 in Figs 2(c) and 3(c). The importance of this effect increases rapidly with increasing velocity amplitude $v_1(z=0)$ of a propagating wave, since the amplitude of the temperature fluctuations increases correspondingly.

Often the effects described above enhance each other. For example, if λ_w is smaller than approximately twice the width of the contribution function, then both an up- and a downflowing part of the wave are always present within the height range of line formation. A temperature-sensitive Fe I line will therefore be preferentially formed in the cooler downflowing part of the wave, so that the line is redshifted at all times and $\Delta\lambda_V^{\max}$ is decreased. An extreme example of this behaviour is shown in Fig. 5. In Fig. 5(a), three Stokes I profiles of line 1, formed along the tube axis, are plotted for a propagating wave with $\lambda_w = 150$ km and $v_1(z=0) = 2.5$ km s^{-1}. The dashed and the dot–dashed profiles correspond to two almost opposite phases, while the solid profile is averaged over a complete wave period. For this wave, the $\Delta\lambda_V(t)$ signal of all the calculated Fe I lines invites the wrong interpretation of a fast stationary downflow within the magnetic feature with a small wave superposed on it (*cf.* the line minimum wavelength). Note also the extremely asymmetric shapes of the line profiles. In the absence of a clear $\Delta\lambda_V(t)$ signal, such an asymmetry may serve to identify large-amplitude tube waves. It is better not to use lines with large Landé factors to diagnose such waves, since the interpretation of their profiles becomes extremely involved due to the interplay of velocity and Zeeman splitting (recall that the field strength is also a function of height and time). As an example, line 6 ($g=3$) is shown in Fig. 5(b). A temperature-insensitive line (e.g. line 5, shown in Fig. 5c) also exhibits only slight variations of the line core.

The time-averaged Stokes V profiles are unshifted for standing waves and practically unshifted for upwards propagating waves with thermal fluctuations switched off ($\gamma = 1$), but are redshifted for propagating waves with $\gamma > 1$.† The redshift increases with increasing wave amplitude v_1, with increasing γ, with decreasing Λ_w and with decreasing excitation potential of the spectral line. It is largest for line 2 and smallest for line 5 (the value for line 3 is unreliable). The $\Delta\lambda_V$ values of the time-averaged Stokes V profiles are in agreement with the observed absence of zero-crossing shifts larger than 0.25 km s^{-1} (Solanki 1986) for propagating waves with $v_1(z=0) \lesssim 1.5$ km s^{-1}, $\gamma < 1.4$ and $\Lambda_w \gtrsim 300$ km. For larger amplitude waves, lines 1 and 2 show too large $\Delta\lambda_V$ values. This suggests that if longitudinal tube waves with large amplitudes are present, then either their temperature fluctuations are smaller than in our calculations (non-linear effects?), or $\Delta\phi$ is closer to 90° than in our calculations (radiative damping).

3.3 Stokes V amplitudes and areas

Fig. 2 demonstrates that the Stokes V wing amplitudes and areas can vary considerably with time. It should therefore also be possible to detect a wave by observing these parameters. For line 3, i.e. for strong temperature-sensitive lines, the measurement of variations in the area or amplitude of a single Stokes V wing or in the Stokes V asymmetry appears to be the method of choice for directly detecting longitudinal tube waves.

By determining the Stokes V wing amplitudes, or areas together with the Stokes V wavelength shift as a function of time, we can observe the influence of the velocity and the temperature concurrently. Note that for weakly Zeeman-split lines, the latter is closely related to the line depth of the Stokes I profile arising from within the magnetic feature (Solanki & Stenflo 1984). Such a measurement is equivalent to the traditional intensity–velocity measurements of acoustic or gravity waves in the quiet Sun (e.g. Schmieder 1978; Deubner & Fleck 1989). It forms another way of deciding between standing or propagating waves, since Stokes V intensity (amplitudes or areas) and velocity have different phase relationships in the two cases.

3.4 Linewidths

The Stokes V profiles observed in active regions and the quiet network show a strong non-thermal, non-magnetic broadening. In the past this broadening has been modelled using a mixture of macro- and microturbulence (e.g. Solanki 1986; Solanki, Keller & Stenflo 1987; Keller *et al.* 1990). However, a considerable fraction of what has classically been described by macro- and microturbulence in the quiet Sun is produced by convective, oscillatory and wave motion (Nordlund 1984). Similarly, we expect the non-thermal, non-magnetic line broadening in flux tubes to be mainly due to

†The net Stokes I profile shifts seen by Eriksen & Maltby (1967) and Maltby & Eriksen (1967) for isothermal propagating waves are probably connected with the very large pressure fluctuations assumed by them.

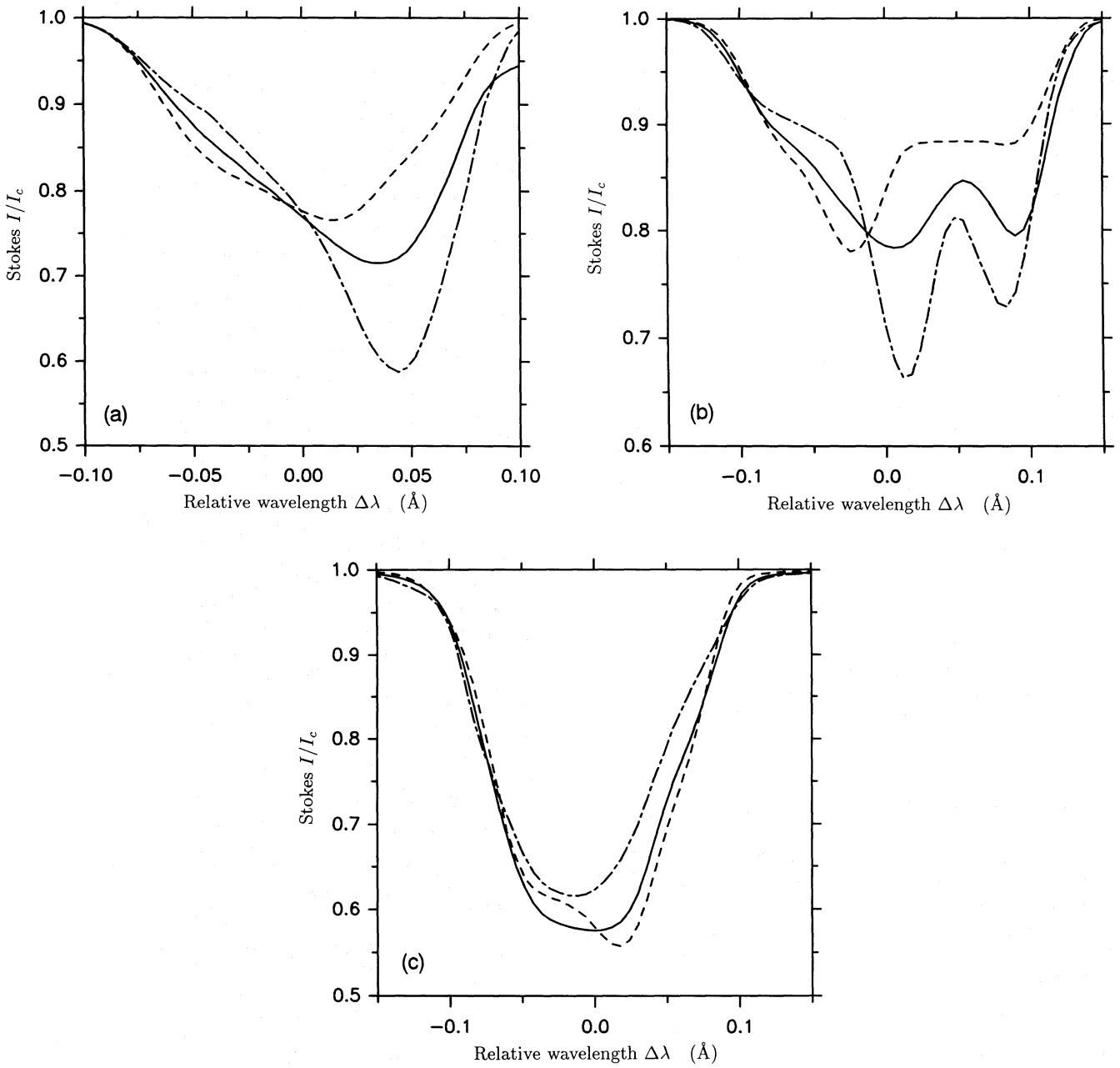

Figure 5. Stokes I/I_c profiles formed along the tube axis in the presence of a propagating tube wave with $v_1(z=0)=2.5$ km s^{-1} and $\Lambda_w=150$ km. Solid curves: Stokes I formed along the central ray integrated over a full wave period. Dashed and dot–dashed curves: Stokes I profiles formed along the central ray at two almost opposite phases of the wave. (a) Line 1. Note the strong asymmetry of this profile and the considerable contribution it appears to obtain from the upflowing parts of the wave at all times. (b) Same as (a), but for line 6. (c) Same as (a), but for line 5.

oscillatory or wave motions, convection being suppressed by the magnetic field (see also Solanki 1989).

We use the term 'Stokes V width', abbreviated as v_D, to denote the wavelength difference between the centres of gravity of the blue and red Stokes V wings. For weakly Zeeman-split lines, this parameter behaves similarly to the width of the integrated V or I_V profile (see Solanki & Stenflo 1984 for more details on the I_V profile) and is also well correlated to the half-width of the Stokes I profile formed along the axis of the flux tube. Although v_D is seen to vary with phase, its variation is generally considerably smaller than the variation of λ_V, λ_r, λ_b and is of small value as a diagnostic of flux tube waves.

Of considerable interest for the presently available observations is v_D of the time-averaged Stokes V profile. We have therefore considered this parameter in detail. For example, we have used an isothermal sine wave to test the reliability of the 'Gaussian micro- and macroturbulence' approximation used in the past to describe the time-averaged line broadening in flux tubes. Not surprisingly we find that if

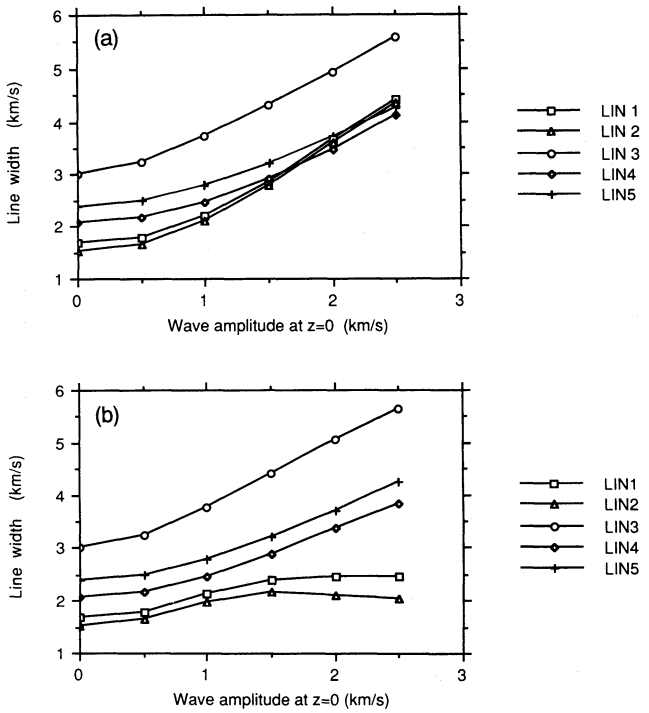

Figure 6. (a) Stokes V linewidths of lines 1–5 as a function of $v_1(z=0)$ for isothermal propagating waves ($\gamma=1$). The static underlying atmospheric model is the network flux tube model. Squares: line 1, triangles: line 2, circles: line 3, diamonds: line 4, plus signs: line 5. (b) As (a), for non-isothermal waves ($\gamma=1.4$).

Λ_w is sufficiently large (i.e. much larger than the width of the contribution function), the linewidths and shapes behave qualitatively as expected from the macroturbulence approximation, while waves with small Λ_w produce a signature similar to microturbulence (*cf.* e.g., Holweger *et al.* 1978). For a simple purely sinusoidal wave with a given amplitude $v_1(0)$ at $z=0$, we empirically obtain the following approximate relationship:

$$v_D^2 \approx [\sqrt{2} v_1(0)]^2 + v_{D_0}^2, \tag{18}$$

where v_{D_0} is the linewidth in the absence of the wave. The factor $\sqrt{2}$ takes into account that larger velocities are more strongly weighted in a sinusoidal wave than in the Gaussian distribution of velocities generally assumed for micro- and macroturbulence.

Fig. 6 shows v_D versus $v_1(0)$ for isothermal (Fig. 6a) and for non-isothermal (Fig. 6b) propagating waves (wavelength of approximately 300 km). Note in particular the behaviour of lines 1 and 2 in the two cases. Interestingly, line 3 is slightly broadened by temperature fluctuations.

One often used method to set an upper limit on the mechanical energy flux is to consider the line broadening (e.g. Athay & White 1978). Obviously, in the presence of non-isothermal waves, the linewidth of temperature-sensitive lines can become an unreliable indicator of the wave amplitude (lines 1 and 2 in Fig. 6b). The present calculations suggest that Fe II lines (such as lines 5 and 8) are likely candidates for setting a relatively reliable upper limit on wave energy flux. Note that unless compensated for, spectral smearing increases the upper limit.

Fig. 6(b) can be explained by the alternate temperature-induced weakening and strengthening of the lines in the hot and cool phases, respectively. For the weak lines (1 and 2) this implies mainly a change in line depth with phase, while for the strong line (3) it means mainly a variation of the linewidth. Since line 1 is greatly weakened in the hot phase, the profile formed during the hot phase makes little contribution to the time-averaged profile, which remains quite narrow, with a width corresponding approximately to the width of the line in the cool phase. The same is true for line 2. For line 3, due to its larger saturation, the increase in width during the cool phase manages to offset the effect of its weakening during the hot phase. To test the above explanation, we have also changed the amplitude of the thermal fluctuations, while leaving the velocity unchanged. The lines satisfy the predictions of the mechanism outlined above. For waves with shorter wavelengths, the behaviour of the linewidths is more complex (*cf.* Fig. 5).

3.5 Stokes V asymmetry

Finally, let us consider how tube waves affect the Stokes V asymmetry. We quantify the asymmetry between the blue and red Stokes V wings by two parameters, the relative area asymmetry δA [defined as $\delta A=(A_b-A_r)/(A_b+A_r)$, where A_b and A_r are the unsigned areas of the blue and red wings of Stokes V, respectively] and the relative amplitude asymmetry δa [defined as $\delta a=(a_b-a_r)/(a_b+a_r)$, where a_b and a_r are the unsigned amplitudes of the blue and red wings of Stokes V respectively]. The Stokes V asymmetry is of particular interest as a diagnostic of the mass motions within and in the immediate surroundings of solar magnetic flux tubes. Since it is the parameter most sensitive to the flux tube geometry, we only discuss the results of the multiray calculations. Due to the low spatial and temporal resolution of the best current observations of Stokes V asymmetry, we are mainly interested in line profiles averaged over a full wave period. The model calculations can be divided into two groups, one with, the other without a downflow v_{ext} in the surrounding of the flux tube. An external downflow has recently been shown to be the major cause of δA (Grossmann-Doerth, Schüssler & Solanki 1988b, 1989; Solanki 1989), but the calculations of Solanki (1989) also demonstrate that the amplitude asymmetry δa resulting from external downflows is too small compared to the observed values. He also showed that non-stationary mass motions within the flux tubes can enhance the δa value. Longitudinal tube waves are an obvious candidate for such motions. We do not expect the calculated profiles from models with $v_{ext}=0$ to give reasonable δA values. Such models serve to illustrate the Stokes V asymmetry produced by tube waves alone. In the other group of models, a height-independent external downflow, with values between 0.5 and 1.5 km s^{-1}, was chosen. The stratification of the external atmosphere is assumed to remain in hydrostatic equilibrium, in keeping with the small v_{ext}/c_s ratio.

Consider first the case of $v_{ext}=0$. Then our calculations show that, due to the absence of a temperature–velocity correlation, standing waves, or isothermal propagating waves, do not produce any net asymmetry in the Stokes V profile averaged over a full wave period. Non-isothermal propagating waves produce only small δA values of 0–3 per

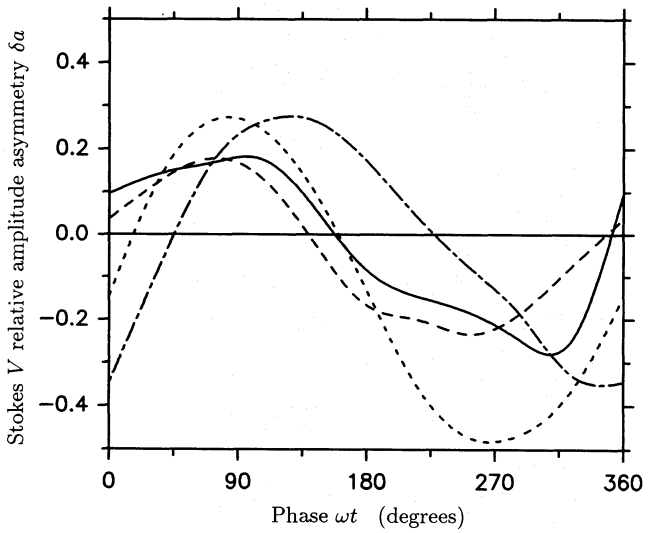

Figure 7. The relative amplitude asymmetry, δa, of Stokes V versus ωt. $\delta a = (a_b - a_r)/(a_b + a_r)$, where a_b and a_r are the unsigned blue and red Stokes V wing amplitudes, respectively. Plotted are line 1 (solid curve), line 3 (dashes), line 5 (short dashes) and line 6 (dot–dashes).

cent for the investigated cases, i.e. $v_1(z=0) \lesssim 1.5$ km s^{-1}. The amplitude asymmetry δa, on the other hand, can be quite substantial (more than 10 per cent for line 3). Averaged over a full wave period, downflowing waves produce a net positive asymmetry (blue wing stronger than red wing), while upflowing waves produce the opposite sign. Thus only downflowing waves are consistent with the observations of positive asymmetry at disc centre.

To understand this behaviour, consider now the variation of δa as a function of phase. It is shown in Fig. 7 for an upwards propagating wave ($\gamma \approx 1.4$). An asymmetry in Stokes V is present at almost every phase and varies considerably with time. The δA and a part of the δa due to the wave is produced by the presence of vertical gradients in the velocity and in the magnetic field (Illing, Landman & Mickey 1975). The change in sign of δa (near phases 0° and 180°, *cf.* Fig. 7) is caused by the change in sign of the velocity gradients at the level of line formation. The behaviour of δA as a function of phase is qualitatively similar to that of δa shown in Fig. 7. In contrast to δA, δa does not simply add linearly together when two or more V profiles are added together. Therefore, the time-averaged δa may be enhanced or lowered relative to the δa of the individual Stokes V profiles (Solanki 1989). The enhancement of δa is largest for temperature-sensitive lines and is mainly due to the temperature–velocity correlation at the height of line formation.

The temperature *in*sensitive lines (lines 4 and 7 and in particular lines 5 and 8) show little net δa or δA when averaged over a full wave period for any of the waves, as long as $v_{ext} = 0$. This is easily understood, since the net Stokes V asymmetry is produced mainly by the difference in profile strength between the upflowing and downflowing phases, and temperature-insensitive lines have virtually the same strength in both phases. In contrast, the observed δA and δa of these lines is of a magnitude similar to that of temperature-sensitive lines. This disagreement effectively rules out linear tube waves as the prime producers of δA in magnetic elements.

The introduction of an external downflow substantially changes the above picture, since large net asymmetries are easily produced. Even for upflowing waves, a positive time-averaged δA can be produced if $v_{ext} \gtrsim 2/3 v_1$. The variation of δa and δA versus phase curves are all shifted in the positive direction by an amount depending on v_{ext}.

Unfortunately, linear tube waves turn out to be disappointing as far as increasing the $\delta a/\delta A$ ratio is concerned. Although we have covered a considerable range of parameters ($0 \lesssim v_{ext} \lesssim 2v_1$ for different waves), we have been unable to enhance sufficiently the $\delta a/\delta A$ ratio of more than at the most two lines in our sample at a time. Since the enhancement of the $\delta a/\delta A$ ratio is also a product of the temperature–velocity correlation, the enhancement is larger for the temperature-sensitive lines than for the Fe II lines if v_1 is larger than v_{ext}. In contrast, the *observed* Fe II lines exhibit a similar $\delta a/\delta A$ ratio to the Fe I lines. The difference between the δa of the synthetic Fe I and II lines decreases as the ratio v_{ext}/v_1 increases, but the influence of the wave on δa also decreases. Therefore, undamped linear tube waves do not appear to be the source of the enhanced Stokes V amplitude asymmetry.

4 CONCLUSION

We have presented linear calculations of undamped magnetoacoustic waves using the thin-tube approximation, and have analysed their influence on the Stokes I and V line parameters of a set of photospheric spectral lines. With a view to improving the observational diagnostics of flux tube waves, the dependence of various line parameters, such as the Stokes V zero-crossing wavelength, Stokes V width, amplitude, area and asymmetry, on wave parameters has been studied in detail. The Stokes I and V profiles are shifted, broadened and generally also distorted by the waves. Such waves are best detected by high spatial resolution time series of Stokes V zero-crossing shifts (of not too strong lines), amplitudes or areas.

We find that it is possible to set a lower limit on the energy flux transported by longitudinal tube waves by measuring time series of the Stokes V zero-crossing wavelength of a selected group of lines. Furthermore, the linewidth of temperature-insensitive lines may be used to set a reliable upper limit on this energy flux.

Propagating magnetoacoustic waves also produce an amplitude asymmetry, but only an insignificant area asymmetry, of the time-averaged Stokes V profiles. The correct sign of the asymmetry is reproduced by downwards propagating waves. In order to produce a substantial area asymmetry, models including both a wave and a downflow in the ambient non-magnetic atmosphere have also been calculated. Depending on the details (external flow velocity, temperature–velocity correlation) these models can produce the correct signs of δA and δa and the approximately correct magnitude of δA. However, these models are still incapable of reproducing the magnitude of the observed $\delta a/\delta A$ ratios, in particular of the temperature-insensitive Fe II lines. In addition, the observed sign of the asymmetry is only produced by downflowing waves. The correlation of magnetic fields with regions of enhanced heating in the lower chromo-

sphere (e.g. Schrijver *et al.* 1989) suggests an excess of upwards propagating waves, carrying energy from the photosphere into the chromosphere. Consequently, the present calculations rule out undamped linear waves as the source of the observed Stokes V area asymmetry or of the enhanced amplitude asymmetry in small-scale magnetic features. Since radiatively damped linear waves also rely on the temperature–velocity correlation to produce an asymmetric Stokes V profile averaged over a wave period, it is unlikely that they will be able to enhance the amplitude asymmetry of temperature-insensitive Fe II lines by the observed amount. Therefore, any large-amplitude longitudinal waves in flux tubes are non-linear, with different up- and downflowing velocity amplitudes, or else the thin-tube approximation breaks down, i.e. the amplitudes of phases of the waves are a function of horizontal position within the flux tubes. An investigation of the influence of non-linear waves, modelled in a very crude manner, on δa and δA by Grossmann-Doerth, Schüssler & Solanki (1991) has produced more promising results.

ACKNOWLEDGMENTS

It is a pleasure to acknowledge helpful discussions on the theoretial aspects of flux tube waves with Manfred Schüssler and on the observational aspects with Bernhard Fleck. One of us (SKS) wishes to thank the members of the St Andrews solar theory group and in particular Eric Priest for making his stay with them so memorable.

REFERENCES

Anderson, L. S. & Athay, R. G., 1989. *Astrophys. J.*, **336,** 1089.
Athay, R. G. & White. O. R., 1978. *Astrophys. J.*, **226,** 1135.
Beckers, J. M., 1969. *Sol. Phys.*, **9,** 372.
Defouw, R. J., 1976. *Astrophys. J.*, **209,** 266.
Deubner, F. L., 1976. *Astr. Astrophys.*, **51,** 189.
Deubner, F. L. & Fleck, B., 1989. In: *High Spatial Resolution Solar Observations, Proc. of the Tenth Sacramento Peak Summer Workshop,* p. 339, ed. von der Lühe, O., National Solar Observatory, Sunspot, New Mexico, USA.
Erikson, G. & Maltby, P., 1967. *Astrophys. J.*, **148,** 833.
Ferriz-Maz, A., Schüssler, M. & Anton, V., 1989. *Astr. Astrophys.*, **210,** 425.
Fleck, B., 1991. *Rev. Mod. Astr.*, **4,** in press.
Gingerich, O., Noyes, R. W., Kalkofen, W. & Cuny, Y., 1971. *Sol. Phys.*, **18,** 347.
Giovanelli, R. G., Livingston, W. C. & Harvey, J. W., 1978. *Sol. Phys.*, **59,** 49.
Godratt, E., Greenfield, A. J. & Schlesinger, Y., 1977. *Cryogenics,* **17,** 81.
Gomez, M. T., Marmolino, C., Roberti, G. & Severino, G., 1987. *Astr. Astrophys.*, **188,** 169.
Grossmann-Doerth, U., Larsson, B. & Solanki, S. K., 1988a. *Astr. Astrophys.*, **204,** 266.
Grossmann-Doerth, U., Schüssler, M. & Solanki, S. K., 1988b. *Astr. Astrophys.*, **206,** L37.
Grossmann-Doerth, U., Schüssler, M. & Solanki, S. K., 1989. *Astr. Astrophys.*, **221,** 338.
Grossmann-Doerth, U., Schüssler, M. & Solanki, S. K., 1991. *Astr. Astrophys.*, **249,** 239.
Gustafsson, B., 1973. *Uppsala astr. Obs. Ann.*, **5,** No. 6.
Hassler, D. M., Rottman, G. J., Shoub, E. C. & Holzer, T. E., 1990. *Astrophys. J. Lett.*, **348,** L77.
Herbold, G., Ulmschneider, P., Spruit, H. C. & Rosner, R., 1985. *Astr. Astrophys.*, **145,** 157.
Heyvaerts, J. & Priest, E. R., 1983. *Astr. Astrophys.*, **117,** 220.
Hollweg, J. V., 1982. *Astrophys. J.*, **254,** 806.
Holweger, H., Gehlsen, M. & Ruland, F., 1978. *Astr. Astrophys.*, **70,** 537.
Illing, R. M. E., Landman, D. A. & Mickey, D. L., 1975. *Astr. Astrophys.*, **41,** 183.
Keil, S. L. & Marmolino, C., 1986. *Astrophys. J.*, **310,** 912.
Keller, C. U., Solanki, S. K., Steiner, O. & Stenflo, J. O., 1990. *Astr. Astrophys.*, **233,** 583.
Knölker, M., Schüssler, M. & Weisshaar, E., 1988. *Astr. Astrophys.*, **194,** 257.
Maltby, P. & Eriksen, G., 1967. *Sol. Phys.*, **2,** 249.
Musielak, Z. A., Rosner, R. & Ulmschneider, P., 1989. *Astrophys. J.*, **337,** 470.
Nordlund, Å., 1984. In: *Small-Scale Dynamical Processes in Quiet Stellar Atmospheres,* p. 181, ed. Keil, S. L., National Solar Obs., Sacramento Peak, New Mexico.
Pantellini, F. G. E., Solanki, S. K. & Stenflow, J. O., 1988. *Astr. Astrophys.*, **189,** 263.
Parker, E. N., 1979. *Cosmical Magnetic Fields,* Clarendon Press, Oxford.
Rae, I. C. & Roberts, B., 1982. *Astrophys. J.*, **256,** 761.
Rammacher, W. & Ulmschneider, P., 1989. In: *Solar and Stellar Granulation, Proc. NATO Advanced Research Workshop,* p. 589, eds Rutten, R. & Severino, G., Reidel, Dordrecht.
Roberts, B., 1984. In: *The Hydromagnetics of the Sun, Proc. Fourth European Meeting on Solar Physics, ESA SP-220,* p. 137, eds Guyenne, T. D. & Hunt, J. J.
Roberts, B., 1986. In: *Small Scale Magnetic Flux Concentrations in the Solar Photosphere,* p. 169, eds Deinzer, W., Knölker, M. & Voigt, H. H., Vandenhoeck & Ruprecht, Göttingen.
Roberts, B., 1990. In: *Proc. Chapman Conference on Magnetic Flux Ropes,* p. 113, eds Russell, C. T., Priest, E. R. & Lee, T. D., American Geophys. Union, Washington.
Roberts, B. & Webb, A. R., 1978. *Sol. Phys.*, **56,** 5.
Roberts, B. & Webb, A. R., 1979. *Sol. Phys.*, **64,** 77.
Ryutova, M. P., 1990. *Solar Photosphere: Structure, Convection and Magnetic Fields, IAU Symp. No. 138,* p. 229, ed. Stenflo, J. O., Kluwer, Dordrecht.
Ryutov, D. D. & Ryutova, M. P., 1976. *Soviet Phys. JETP,* **43,** 491.
Schmieder, B., 1978. *Sol. Phys.*, **57,** 245.
Schrijver, C. J., Coté, J., Zwaan, C. & Saar, S. H., 1989. *Astrophys. J.*, **337,** 964.
Schüssler, M., 1990. *Habilitationsschrift,* Universität Göttingen.
Skumanich, A., Smythe, C. & Frazier, E. N., 1975. *Astrophys. J.*, **200,** 747.
Solanki, S. K., 1986. *Astr. Astrophys.*, **168,** 311.
Solanki, S. K., 1987. *PhD thesis,* No. 8309, ETH, Zürich.
Solanki, S. K., 1989. *Astr. Astrophys.*, **224,** 225.
Solanki, S. K. & Stenflo, J. O., 1984. *Astr. Astrophys.*, **140,** 185.
Solanki, S. K. & Stenflo J. O., 1986. *Astr. Astrophys.*, **170,** 120.
Solanki, S. K. & Steenbock, W., 1988. *Astr. Astrophys.*, **189,** 243.
Solanki, S. K. & Roberts, B., 1990. In: *Proc. Chapman Conference on Magnetic Flux Ropes,* p. 181, eds Russell, C. T., Priest, E. R. & Lee, T. D., American Geophys. Union, Washington.
Solanki, S. K., Keller, C. & Stenflo, J. O., 1987. *Astr. Astrophys.*, **188,** 183.
Spruit, H. C., 1981. *Astr. Astrophys.*, **98,** 155.
Spruit, H. C. & Roberts, B., 1983. *Nature,* **304,** 401.
Steiner, O. & Pizzo, V. J., 1989. *Astr. Astrophys.*, **211,** 447.
Stenflo, J. O., 1989. *Astr. Astrophys. Rev.*, **1,** 3.
Stenflo, J. O. & Harvey, J. W., 1985. *Sol Phys.*, **95,** 99.

Thomas, J. H., 1985. In: *Theoretical Problems in High Resolution Solar Phsics,* p. 126, ed. Schmidt, H. U., Max Planck Institute for Astrophysics, Munich.
Van Ballegooijen, A. A., 1985. In: *Measurements of Solar Vector Magnetic Fields,* p. 322, ed. Hagyard, M. J., NASA Conf. Publ. 2374.
Webb, A. R. & Roberts, B., 1980. *Sol. Phys.,* **68,** 87.
Wentzel, D. G., 1974. *Sol. Phys.,* **39,** 129.
Wiehr, E., 1985. *Astr. Astrophys.,* **149,** 217.
Zayer, I., Solanki, S. K. & Stenflo, J. O., 1989. *Astr. Astrophys.,* **211,** 463.